

# Hierarchical Cluster Assembly in Globally Collapsing Clouds

Enrique Vázquez-Semadeni<sup>1\*</sup>, Alejandro González-Samaniego<sup>2</sup>, and Pedro Colín<sup>1</sup>

<sup>1</sup>*Instituto de Radioastronomía y Astrofísica, Universidad Nacional Autónoma de México, Apdo. Postal 3-72, Morelia, 58089, México*

<sup>2</sup>*Center for Cosmology, Department of Physics and Astronomy, University of California at Irvine, Irvine, CA 92697, USA*

2 November 2016

## ABSTRACT

We discuss the mechanism of cluster formation in a numerical simulation of a molecular cloud (MC) undergoing global hierarchical collapse (GHC), to understand how the gas motions in the parent cloud control the assembly of the cluster. The global nature of the collapse implies that the star formation rate (SFR) increases over time. The “hierarchical” nature of the collapse consists of small-scale collapses within larger-scale ones. The large-scale collapses culminate a few Myr later than the small-scale collapses and consist of filamentary flows that accrete onto massive, dense central clumps. In turn, the small-scale collapses form clumps embedded in the filaments, that are falling onto the central clump assembled by the ongoing large-scale collapse. The stars formed in the early, small-scale collapses share the infall motion of their parent clumps towards the larger-scale potential well, so that the filaments feed both gaseous and stellar material to the massive central clump. This leads to the presence of a few older stars in a region where new protostars are forming at a higher rate, and also to a self-similar or fractal-like structure of the clusters, in which each unit is composed of smaller-scale sub-units, which approach each other and may eventually merge, explaining the frequently-observed morphology of cluster-forming regions. Moreover, because the older stars formed in the filaments share the infall motion of the gas onto the central clump, they tend to have larger velocities and to be distributed over larger areas than the younger stars formed in the central clump, where the gas from which they form has been shocked and has dissipated some kinetic energy. Finally, interpreting the IMF as a probability distribution, so that the probability of forming a massive star is much lower than that of forming a low-mass one, implies that massive stars only form once the *local* SFR is large enough to sample the IMF up to high masses. In combination with the increase of the SFR, this implies that massive stars tend to appear late in the evolution of the MC, and only in the central massive clumps. We discuss the correspondence of these features with observed properties of young stellar clusters, finding very good qualitative agreement, thus providing support to the scenario of global, hierarchical collapse of MCs, while explaining the origin of the observed cluster structure.

**Key words:** Galaxies: star clusters, Gravitation, Hydrodynamics, ISM: clouds, Stars: formation

## 1 INTRODUCTION

It is presently accepted that most stars form in clusters or groups, although the details of the cluster-formation process, especially the origin of their structural properties, remain a matter of active research (see, e.g., the reviews by Lada & Lada 2003; Portegies Zwart et al. 2010; Moraux 2016). In particular, in recent years, a number of struc-

tural properties of the clusters have been uncovered that still require an adequate theoretical understanding, such as: i) The existence of a mass segregation in the clusters, with the most massive stars lying closer to the cluster’s center (Hillenbrand & Hartmann 1998); ii) the distribution of protostellar separations, which appears to have no characteristic scale (Bressert et al. 2010); iii) the likely existence of an age gradient in clusters, with the youngest stars being located in the highest-density regions (Kuhn et al. 2015a); iv) the

\* e-mail: e.vazquez@crya.unam.mx

apparent deficit of OB stars in some infrared dark clouds (IRDCs; Povich et al. 2016).

Numerical simulations have begun to offer some insight about these properties. Kirk et al. (2014) have concluded, from a suite of simulations of self-gravitating, decaying isothermal turbulence, that the most massive stars form in situ at the cluster centers, rather than “sinking” there through dynamical interactions in the cluster itself. However, they gave no physical explanation as to why the most massive stars should form there. More recently, Kuhn et al. (2015b) have suggested, by comparing multi-wavelength observations of stellar clusters with numerical simulations, that clusters form by mergers of “subcluster” structures, although again no explanation of why such mergers should occur is provided (see also McMillan et al. 2007; Allison et al. 2009; Moeckel & Bonnell 2009, for N-body studies of subcluster merging). Observationally, the presence of subunits of somewhat different ages in the clusters has also been pointed out by Rivera-Gálvez et al. (2015).

A physical mechanism capable of providing a unifying scenario to these properties is that of global, hierarchical molecular cloud collapse, advanced by Vázquez-Semadeni et al. (2009, see also Gómez & Vázquez-Semadeni 2014). The latter authors noted that, if molecular clouds (MCs) are assembled by large-scale colliding streams of warm, atomic gas that rapidly condenses into the cold atomic phase, then they quickly become Jeans-unstable and begin to collapse globally. Moreover, the turbulence induced by the collision of the streams causes moderately supersonic turbulence (e.g., Koyama & Inutsuka 2002; Heitsch et al. 2005) in the cold gas, which produces a multi-scale spectrum of density fluctuations, where small-scale, large-amplitude (SSLA) density fluctuations are superposed on larger-scale, smaller-amplitude (LSSA) ones (e.g., Kim & Ryu 2005). Since these density fluctuations are nonlinear, the denser SSLA fluctuations have shorter free-fall times than the LSSA ones, therefore completing their collapse earlier. This process is therefore similar to Hoyle (1953) fragmentation, except that the density fluctuations are of turbulent origin and therefore nonlinear. In this sense, the process is also similar to the mechanism of “gravoturbulent fragmentation” (e.g., Mac Low & Klessen 2004; Ballesteros-Paredes et al. 2007, and references therein), except that the cloud is *not* globally supported by turbulence, and the turbulent fluctuations do not collapse directly, but rather just plant the seeds for subsequent, local, scattered collapses as the cloud contracts globally (Clark & Bonnell 2005). In what follows, we will refer to this intermediate scenario between Hoyle and gravoturbulent fragmentation as “global hierarchical collapse” (GHC).

This scenario also predicts that the star formation rate (SFR) in MCs evolves (initially increasing) over time, as a consequence of the increase of the mean density of the clouds as they go through global gravitational collapse (Zamora-Avilés et al. 2012; Hartmann et al. 2012; Zamora-Avilés & Vázquez-Semadeni 2014). Assuming that massive stars do not form until the SFR is high enough that the IMF is sampled up to high masses, then massive stars form late in the global process, and when they do, they begin to disrupt their parent clouds through their feedback (winds, ionising radiation, SN explosions), reducing the SFR again (e.g.,

Vázquez-Semadeni et al. 2010; Zamora-Avilés et al. 2012; Colín et al. 2013; Zamora-Avilés & Vázquez-Semadeni 2014; Dale et al. 2014, 2015; Gatto et al. 2016).

Gómez & Vázquez-Semadeni (2014) presented a smoothed-particle hydrodynamics (SPH) numerical simulation of cloud formation and evolution in the context of GHC that showed the formation of filamentary structures with embedded clumps. In that simulation, the filaments constitute river-like structures, through which material flows from the extended cloud environment to the dense cores where star formation occurs. When the filaments are sufficiently dense, fragmentation occurs within them as the gas flows along them into the most massive cores. This implies that the filaments supply the dense cores with a mixture of stars and gas.

This kind of flow was also observed (although it was not discussed) in a similar simulation presented by Colín et al. (2013, hereafter Paper I) using the adaptive mesh refinement code ART (Kravtsov et al. 1997, 2003) that included a simplified treatment of radiative transfer and a prescription to form stellar particles<sup>1</sup> (SPs) that allows imposing a power-law SP mass function with a slope similar to that of Salpeter (1955). This implies that, contrary to the situation in the simulation by Gómez & Vázquez-Semadeni (2014), the clusters formed in the simulation of Paper I, as well as their surrounding gas, are subject to realistic dynamics, which allows investigating the evolution of the clusters from their formation to the time when they disperse their surrounding gas.

There exist many numerical studies of cluster formation, focusing on issues such as their stellar mass function, the correlation function of the spatial stellar distribution and cluster boundedness, and the formation of binaries (e.g., Klessen & Burkert 2001; Bate et al. 2003; Bate 2009a); the effect of feedback on producing massive stars (e.g., Bate 2009b; Krumholz et al. 2010, 2012) and on destroying their parent clumps (e.g., Vázquez-Semadeni et al. 2010; Dale et al. 2012, 2013a,b, Paper I); and the energy balance and rotation of the cluster as a function of the initial turbulence level in the parent cloud (Lee & Hennebelle 2016).

In this work, instead, we aim to describe the process of assembly and early evolution of the clusters as a consequence of GHC. To this end, we study a cluster formed in the simulation labeled LAF1 in Paper I, focusing on the resulting spatial structure of the cluster. In Sec. 2 we briefly describe the numerical simulation, and in Sec. 3 we describe the criteria for defining the cluster and stellar groups, both in terms of the origin of their members as well as from their instantaneous positions. Next, in Sec. 4 we present our results concerning the assembly from subunits brought in by the GHC, as well as the resulting structure of the clusters. In Sec. 5 we discuss the implications of our results and compare them with existing observations, and in Sec. 6 we give a summary and some conclusions.

<sup>1</sup> We refrain from calling the stellar particles “sinks” because, contrary to the standard practice for sink particles, our stellar particles are not allowed to accrete. Instead, in our prescription, the accretion is done in the gas phase (cf. Sec 2.3).

## 2 THE NUMERICAL MODEL

The numerical simulation used in this work comes from the set performed in Paper I with the hydrodynamics+N-body Adaptive Refinement Tree (ART) code of Kravtsov et al. (2003). The physical processes included are self-gravity, parameterized heating and cooling (Sec. 2.2), star formation with an imposed but realistic IMF (Sec. 2.3), and simplified radiative transfer for the feedback from massive-star ionising radiation (Sec. 2.4). Magnetic fields are neglected. For more details, we refer the reader to Paper I.

### 2.1 The numerical box and resolution

The simulation represents the head-on collision of two cylindrical streams in the warm neutral medium. The streams each have a radius of 64 pc and a length 112 pc, and each is traveling at a speed of  $5.9 \text{ km s}^{-1}$ . The numerical box (including the streams) initially has a uniform density  $n = 1 \text{ cm}^{-3}$  and temperature  $T = 5000 \text{ K}$ , implying an adiabatic sound speed of  $7.4 \text{ km s}^{-1}$ . Thus, the streams move with a Mach number of 0.8 with respect to the sound speed in the initial uniform background medium.

The simulation uses a base resolution of  $128^3$  grid cells, and allows for 5 refinement levels, reaching a maximum resolution equivalent to  $4096^3$ , with a minimum cell size of 0.0625 pc, or  $\approx 13\,000 \text{ AU}$ . The refinement is based on a “constant mass” criterion, so that a cell size is refined when its mass exceeds  $0.32M_{\odot}$ . This implies that the grid cell size  $\Delta x$  scales with density  $n$  as  $\Delta x \propto n^{-1/3}$ . Once the maximum refinement level is reached, no further refinement is performed, and the cell’s mass can reach much larger values because of the probabilistic SF scheme (Sec. 2.3).

Note that this constant-cell-mass refinement criterion does not conform to the so-called *Jeans criterion* (Truelove et al. 1997) of resolving the Jeans length with at least 4 grid cells. Those authors cautioned that failure to do this might result in spurious, numerical fragmentation. However, we do not consider this a cause for concern since, as will be described in Sec. 2.3, our star formation prescription allows us to choose the stellar-particle mass distribution, and tune it to a Salpeter (1955) value.

### 2.2 Heating and Cooling

We use heating ( $\Gamma$ ) and cooling ( $\Lambda$ ) functions of the form

$$\Gamma = 2.0 \times 10^{-26} \text{ erg s}^{-1} \quad (1)$$

$$\frac{\Lambda(T)}{\Gamma} = 10^7 \exp\left(\frac{-1.184 \times 10^5}{T + 1000}\right) + 1.4 \times 10^{-2} \sqrt{T} \exp\left(\frac{-92}{T}\right) \text{ cm}^3. \quad (2)$$

These functions are fits to the various heating and cooling processes considered by Koyama & Inutsuka (2000), as given by equation (4) of Koyama & Inutsuka (2002), with the typographical corrections noted in Vázquez-Semadeni et al. (2007). With these heating and cooling laws, the gas is thermally unstable in the density range  $1 \lesssim n \lesssim 10 \text{ cm}^{-3}$ . No chemistry tracking is performed, and so the gas is assumed to be all atomic, with a mean particle weight  $\mu = 1.27$ .

### 2.3 Star formation

Our simulation employs a probabilistic star formation prescription such that, if a grid cell reaches a number density  $n > n_{\text{SF}}$ , where  $n_{\text{SF}}$  is a density threshold, then an SP of fixed mass  $m_{\text{SP}}$  may be placed in the cell with a probability  $P$  every timestep of the root (coarsest) grid. If the SP is created, it acquires half of the gas mass of the parent cell.

Unlike standard sink particles (e.g., Bate et al. 1995; Jappsen et al. 2005; Vázquez-Semadeni et al. 2007; Federrath et al. 2010), our SPs do not accrete. However, since our prescription for SF is probabilistic, once the highest refinement level is reached in a cell, it actually continues to accrete from the surrounding material, and grows in mass and density until an SP is actually placed in it. This implies that the accretion is performed in the gas phase, rather than onto the particles. Serendipitously, it was found in Paper I that this prescription allows the SPs to form with a power-law mass distribution, whose slope can be tuned by varying the value of  $P$ , at a given maximum resolution. In Paper I it was reported that setting  $P = 3 \times 10^{-3}$  at the resolution used in our simulation caused the SP power-law mass distribution to attain an exponent of  $-1.34$ , thus being similar to the classical Salpeter value. We set the threshold density for SP formation at  $n_{\text{SF}} = 9.2 \times 10^4 \text{ cm}^{-3}$ , which corresponds to a cell mass of  $0.78M_{\odot}$  at the highest refinement level. Thus, the minimum possible SP mass is  $m_{\text{SP}} = 0.39M_{\odot}$ . With this prescription, the most massive SP formed in this simulation has  $m_{\text{SP}} = 61 M_{\odot}$ .

Note, however, that our imposed IMF is a strict power law, and thus the most probable stellar mass is also the minimum. This implies that we are missing the low-mass ( $M < 0.39M_{\odot}$ ) side of the actual IMF, implying that we are missing about half of the total number of stars, and that their corresponding mass (20–30% of the total mass) is deposited instead into the stars that do get formed in the simulation. We discuss the implications of this in Sec. 5.3.

Our simulation thus contains SPs that represent individual stars (not clusters or groups), with a realistic mass distribution above the most probable stellar mass. This allows the dynamics of the SPs to be reasonably representative of the forming cluster dynamics, contrary to the case when the particles’ masses correspond to those of small groups, of up to a few hundreds of solar masses. In that case, low-mass particles can suffer exceedingly strong encounters with the massive particles, and thus acquire unrealistically high velocities.

### 2.4 Feedback prescription

In our simulation, the feedback effect of the ionising stars on the MC is non-local, using a simplified radiative transfer prescription to model the formation and evolution of a HII region around an SP. As a zeroth-order approximation, we assume a uniform “line-of-sight” (LOS) characteristic density  $n_{\text{LOS}}$  in the HII region, with a value equal to the geometric mean between the density of the cell containing the SP and that of the target cell. Moreover, for any given star we assume an ionising flux  $S_*$  taken from the tabulated data provided by Díaz-Miller et al. (1998). We then compute the corresponding Strömgren radius,  $R_S$ , given by

$$R_S \equiv \left( \frac{3}{4\pi} \frac{S_*}{\alpha n_{\text{LOS}}^2} \right)^{1/3}, \quad (3)$$

where  $\alpha = 3.0 \times 10^{-13} \text{ cm}^3 \text{ s}^{-1}$  is the hydrogen recombination coefficient.

At each time step, we search for all cells surrounding every SP particle whose distances to it are smaller than  $R_S$ . For each target cell that satisfies this condition, we set its temperature to  $10^4 \text{ K}$  and turn off the cooling there. The cell will remain so during the whole lifetime of the star, which is determined by its mass  $m_*$  as

$$t = \begin{cases} 2 \text{ Myr} & \text{if } m_* \leq 8M_\odot; \\ 222 \text{ Myr} \left( \frac{m_*}{M_\odot} \right)^{-0.95} & \text{if } m_* > 8M_\odot. \end{cases} \quad (4)$$

As explained in Paper I, for stars more massive than  $8M_\odot$ , this time is a fit to the stellar lifetimes by Bressan et al. (1993), while for stars with masses lower than that, it represents the fact that the duration of the stellar-wind phase is  $\sim 2 \text{ Myr}$ , roughly independently of mass. This also means that we are representing the effect of the winds and outflows of low mass stars by an ionization prescription. While this is clearly only an approximation, we do not expect it to have much impact on our calculations, since the main source of feedback energy at the level of GMCs is the ionization feedback from massive stars (Matzner 2002).

Although highly simplified, this prescription was tested in Paper I against the known analytic formula for the evolution of  $R_s$  in a uniform medium (Spitzer 1978) and shown to agree within 30%. This, we believe, is accurate enough given our interest in large-scale molecular cloud evolution and the associated cluster dynamics at early stages of assembly, rather than on the structural details of the ionised regions.

### 3 CLUSTER DEFINITION: MEMBERSHIP

One crucial step for the present study is the membership of stars to a given group or cluster. We now discuss our procedure of choice.

Observationally, the identification and membership definition of embedded stellar clusters is intrinsically a complex task, complicated by ambiguities and uncertainties, since the clusters do not have well defined edges, contamination by field stars is difficult to quantify, and faint members may be difficult to identify (e.g., Lada & Lada 2003). In our case, the origin of the stars in the simulations is known, and this allows a classification of the stars by site of origin. However, this information is unavailable to observations, which instead must proceed by first identifying the cluster as a stellar surface density excess, and then define its members mainly on a statistical basis, by comparison with star counts in nearby control fields off the cluster (Lada & Lada 2003). On the other hand, in the simulation there are no “field” stars, but only stars from clusters formed at some other locations in the cloud.

For the purpose of defining a cluster or group<sup>2</sup> by loca-

<sup>2</sup> We use the terms “cluster” and “group” in a somewhat loose way to respectively denote larger and smaller associations of stars, the latter usually being part of the former. The looseness comes

tion at early times, we use the well known friends-of-friends (FOF) algorithm (Davis et al. 1985). This is convenient at early stages, when the first groups of stars are well separated and the stars are easy to tag as part of a group that has formed at a certain time and location. However, note that, because of the hierarchical structure of the clusters,<sup>3</sup> the number and stellar content of the resulting groups depends on the value of the so-called “linking parameter” passed to the algorithm. This parameter is a measure of the distance out to which neighbors are searched. At early times, the separation between groups is easily determined by eye, and the linking parameter can then be chosen to match the visual classification.

At later times, however, the groups change their size by dynamical interactions between their members, and moreover new stars continue to form in the same region, or in its outskirts, making it necessary to suitably define the regions’ size in order to determine stellar membership to a group. We thus define the radius of a group at a given time by performing an iterative process:

(i) Considering only the stars that were part of the group in the previous snapshot, we measure the distance from their center of mass to the most distant star. If this distance is less than twice the distance from the center to the second most distant star, we consider the distance to the most distant star as the radius of the group. Otherwise, we consider the most distant star as a “runaway star” and take the radius of the group as the distance from its center to the second most distant star.

(ii) Next, we assign the new stars (those formed in the period of time between the actual snapshot and the previous one) to the group whose center of mass is closest to them.

(iii) Finally, including the new stars, we recompute the center of mass, size ( $R_g$ ), total mass ( $M_g$ ), and total number of stars ( $N_g$ ) of the group. We also compute the age of the group,  $t_{\text{age}}$ , as the time elapsed since the moment when the group was first defined.

However, neighbouring groups generally approach each other (as part of the large-scale collapse) and often they merge. We say that a new group has formed by the merger of two former groups when the distance between their centers of mass is smaller than the larger of the two radii. At that point, we consider that the earlier subgroups disappear. In general, we expect this process to operate at all scales in our simulation, with groups in turn forming from subgroups, and so on, in a hierarchical and self-similar manner.

## 4 RESULTS

### 4.1 Global evolution and hierarchical cluster assembly

In this simulation, three main clusters form, two of which are sufficiently massive to clear out the dense gas around them

from the fact that, given the hierarchical and evolutionary nature of the process, both clusters and groups evolve and grow in stellar count, mass and size.

<sup>3</sup> In our simulation, stars are born naturally in groups and subgroups; see Secs. 1 and 4.

on a timescale  $\tau_{\text{clear}} \sim 17$  Myr since the formation of the first stars (from  $t \sim 19$  Myr to  $t \sim 36$  Myr in the evolution of the simulation). Stars begin to form at  $t \approx 18.9$  Myr, and the first HII regions appear at  $t \approx 24.2$  Myr.<sup>4</sup> Specifically, at  $t \approx 37.5$  Myr, the dense gas has been cleared from a radius of  $\sim 70$  pc around the clusters. Figure 1 shows one snapshot of the simulation, at  $t = 25.90$  Myr into the evolution, in which two HII regions, surrounding the two most massive clusters, can be seen, while the filamentary structure of the cloud is still noticeable in general. The clusters themselves have formed along the main filamentary structures in the cloud, and contain  $10^3$ – $10^4 M_{\odot}$ . Note also that the structure of the most massive cluster retains the filamentary shape of its parent cloud, similarly to, for example, the structure observed in the Orion A cloud (see, e.g., Fig. 1 of Hacar et al. 2016). This similarity in fact is not limited to the filamentary shape, but also includes the fact that the filament has a larger concentration of stars in one end. In a future paper we plan to quantitatively explore the structure and kinematics of these observed and simulated clusters.

The crucial effect of the GHC scenario is that the filaments constitute part of the large-scale gravitational collapse, funneling gas into the cores within them, as observed by Gómez & Vázquez-Semadeni (2014) in a numerical simulation of cloud formation and collapse. Moreover, these authors observed a hierarchy of collapses within the filaments, so that *small clumps, which are collapsing locally, and sometimes forming stars already, are themselves falling onto larger-scale ones*, similarly to the “conveyor belt” scenario proposed by Longmore et al. (2014) for the gas stream in the Central Molecular Zone. This is illustrated in Fig. 2, which shows a series of snapshots around the second most massive cluster (hereafter, “Cluster 2”, located in the upper left part of the cloud) among those seen in Fig. 1, from  $t = 18.92$  Myr to  $t = 22.40$  Myr. From  $t = 18.92$  to 19.05 Myr it can be seen that new stars have formed in the first group. At  $t = 19.35$  Myr, a second group is seen to have formed at a distance  $\sim 2.5$  pc from the first. By  $t = 21.14$  Myr, this second group is seen to have approached the first, being at a distance  $\sim 1.5$  pc from it, and to have merged with it by  $t = 21.70$  Myr. Also, at this time, a third group is seen to begin forming in the far left part of the filament, containing only one star at that time, although by  $t = 22.83$  Myr it already contains several stars (not shown).

The effect of the feedback is also worth noting. Already by  $t = 21.14$  Myr, the section of the filament connecting the two clusters is seen to be partially disrupted, and some gas is being expelled from the clump containing the main group. However, accretion along the filament is seen to have replenished this section of the filament at  $t = 21.70$  Myr, although the other side of the filament is now seen to be in the process of dispersal. Finally, by  $t = 22.40$  Myr, the

filament is seen to be in the process of dispersal on both sides of the cluster.

Figure 3 then shows the late stages of the evolution of this cluster. By  $t = 24.37$  Myr the filament is seen to have been dispersed out to distances  $\sim 10$  pc, and by  $t = 25.62$  Myr, a large HII region, of diameter  $\sim 15$  pc has formed, although the group on the left retains some of its gas, and a new group has formed in an “pillar” that constitutes the remainder of the filament. Also, along this filamentary structure, yet another group is seen to have formed (at the far right of the image). By  $t = 27.02$  Myr, most of the dense gas has been cleared from the region, and the cluster is seen to consist of four groups, two of them almost devoid of gas (“naked”) and two of them still embedded in their respective clumps.

From the above description, it becomes clear that the clusters in this simulation are assembled by means of a hierarchical process, in which subunits formed at slightly different locations and times merge as they fall into a large-scale potential well, *feeding the central clump with both stars and gas*. In the following sections we discuss various implications of this mechanism.

## 4.2 Subgroup evolution and merger

The resulting evolution of Cluster 2 is illustrated in Fig. 4, which shows the projected positions of the stellar particles on the  $(x, y)$  plane at times  $t = 20.59, 21.44, 22.40,$  and  $25.34$  Myr in the *top left, top right, bottom left, and bottom right panels*, respectively.

In this cluster, stars begin to form at  $t \approx 19.2$  Myr and Fig. 4 shows that they are assembled into a cluster in such a way that at  $t = 20.59$  Myr we identify two subgroups (hereafter, Groups 1 and 2; see the *top left panel* of Fig. 4) of what will later become a larger, merged group (Group 1-2). We use square symbols to identify stars that belong to Group 1, and filled circles for stars belonging to Group 2. Furthermore, we color them according to their age as shown in the labels and qualitatively represent their masses by the symbol size, with larger symbols indicating larger masses. The green and red circles represent the group radii at each time, computed as explained in Sec. 3, with the dashed circles representing the size out to the most distant star, and the solid circles representing the distance to the second most distant star. In what follows, we use the distance to the second most distant star as the radius of Group 1-2, because the first most distant one is clearly “running away” from the group. Finally, we use larger symbols to represent more massive stars, and smaller symbols to represent lower-mass stars. Thus, even at these early stages, we can see that *the more massive and younger stars tend to be near the centers of the groups*.

From Fig. 4 it is clearly seen that, at these early stages, the groups are undergoing expansion, and that star formation continues within them. By  $t = 21.44$  Myr, both groups have similar sizes, masses, and number of stars, and they have undergone a large enough expansion that their merger appears inevitable. The formerly “most distant” star of Group 2 is now far away from the center of either group. By our definition, the merger occurs at  $t = 21.56$  Myr, forming the new Group 1-2. We have kept the circular and square symbols to indicate the original group membership of the

<sup>4</sup> Here, it is important to recall that the GHC scenario implies that the first episodes of SF involve small numbers of stars, and thus they do not manage to sample the IMF out to large stellar masses. The early SF episodes occur in a “scattered” mode, which corresponds to the culmination of the collapse of the low-mass, high-density, small-scale (SSLA) fluctuations that produce low numbers of stars, and that are themselves falling into the large-scale potential wells that later become the high-mass SF sites (Vázquez-Semadeni et al. 2009).

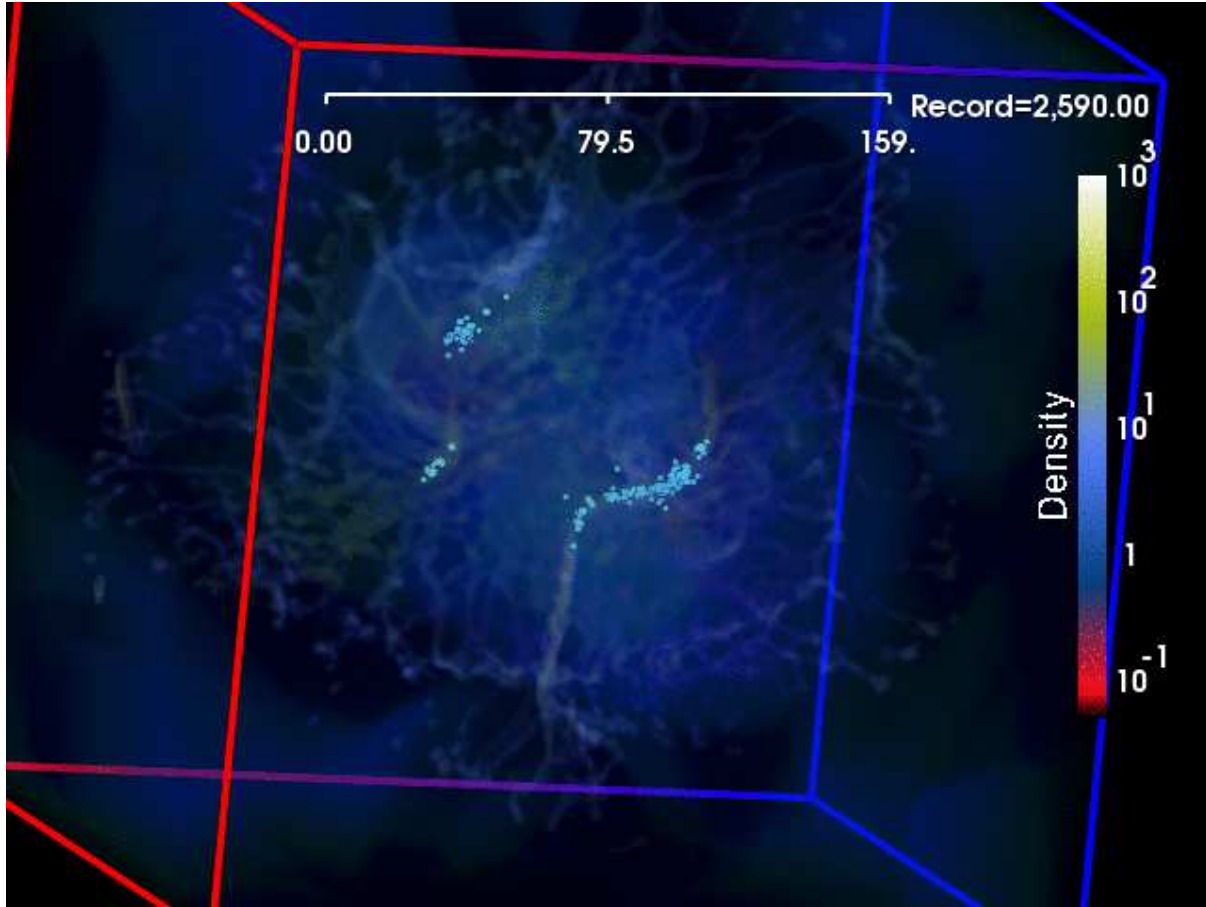


**Figure 1.** A global projected view at  $t = 25.9$  Myr, showing the three clusters that form within filamentary structures. The box size is 256 pc and the ruler shows a scale of 159 pc. The color bar indicates the local density in  $\text{cm}^{-3}$ . The cyan dots represent individual stars. Expanding shells can be seen around the two most populous clusters.

stars in the merged group. Triangles now represent stars born in the new Group 1-2. Thus, this new group contains stars that were born at somewhat different times and locations.

For later times, we continue to track the evolution of this and other, new groups appearing in a 10-pc box around Group 1-2, and by  $t = 25.34$  Myr, we now find a system of groups with different ages, masses, and sizes (*bottom right panel* of Fig. 4). These groups lie approximately in a straight line, because they formed in the filament feeding the main clump. Eventually, as these groups expand and approach each other, they finally become part of what we refer to as the whole Cluster 2, as seen in the *bottom right panel* of Fig. 3, although the subunits are still partially distinguishable at that time ( $t = 29.96$  Myr).

#### 4.3 Star formation rate and delayed massive-star formation

As mentioned in the Introduction, one fundamental implication of the GHC scenario is that the SFR of star-forming clouds must increase in time until the time when massive stars begin to appear and to destroy their parent MC (Zamora-Avilés et al. 2012; Zamora-Avilés & Vázquez-Semadeni 2014). Figure 5 shows

the evolution of the SFR in Groups 1 and 2, as well as in the merged Group 1-2. Except for Group 2, in whose parent cloud the SFR starts relatively high and then decreases, for Groups 1 and 1-2 the trend of increasing SFR is observed. Moreover, the SFR for the merged Group 1-2 is much larger than the maximum value reached in Group 2 before the merger, so the increase of the SFR also holds for the system of Groups 1 and 2 combined, before and after their merger.

Assuming that massive stars do not form in a region until the SFR is locally high enough to sample the IMF up to large masses, the increase of the SFR implies that the massive stars should tend to appear late in the evolution of star-forming regions. This is illustrated in Fig. 6, which shows the mass of the stars *vs.* their age at  $t = 22.40$  and  $t = 23.66$  Myr. At both times, it is clearly seen that the oldest stars have the lowest masses, and that, as the age decreases, the range of stellar masses extends to larger values.

This is also illustrated in Fig. 7, which shows the cumulative mass distribution of Groups 1, 2, and 1-2 at various times. It is seen from this figure that the relative abundance of massive stars increases over time, especially after Groups 1 and 2 have merged.



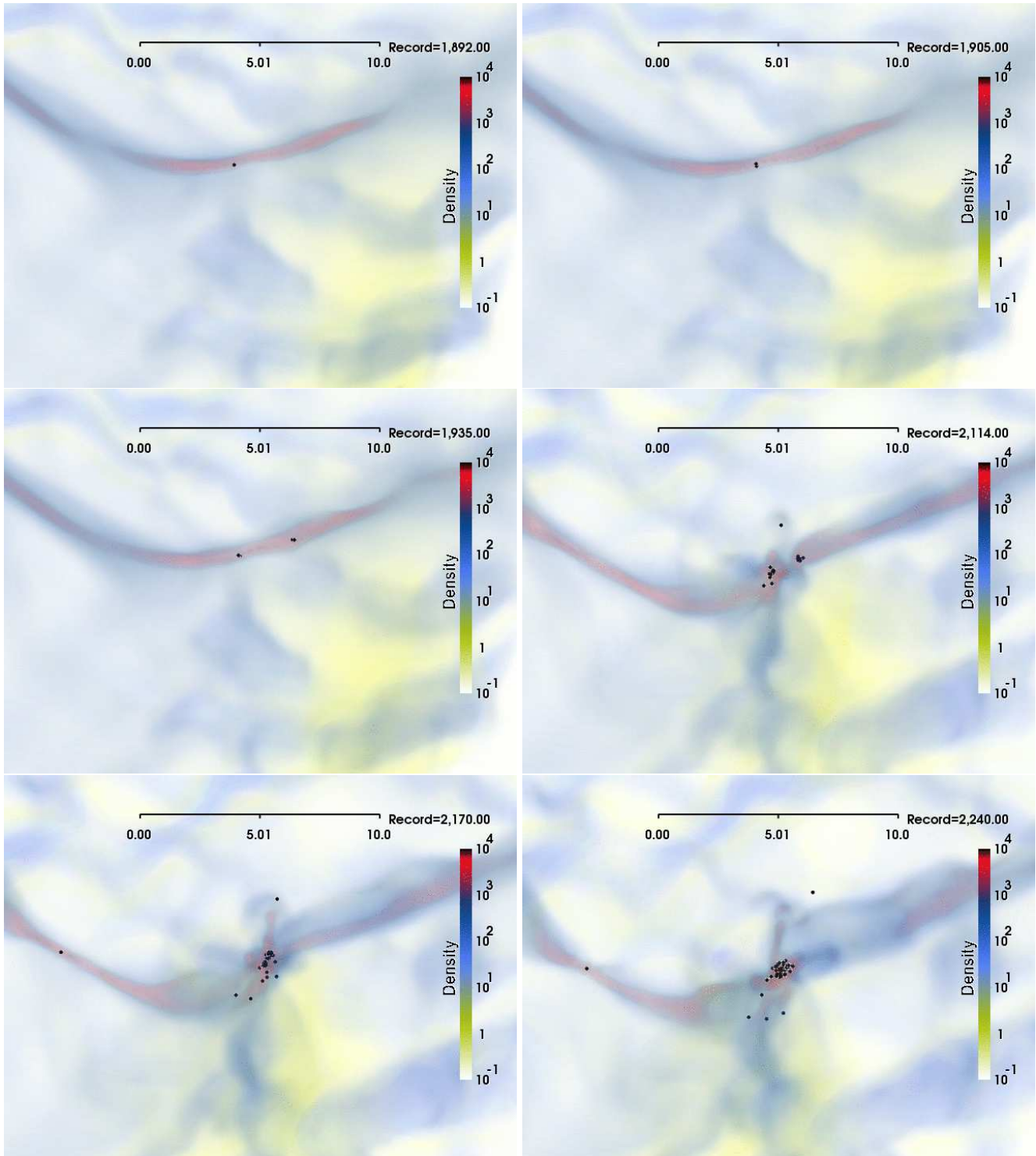


**Figure 2.** Six projected images zooming in around the intermediate-mass cluster at  $t = 18.92, 19.05, 19.35, 21.14, 21.70,$  and  $22.40$  Myr, showing the hierarchical assembly of the cluster by the merging of groups that form along a filament, which feeds the main clump. The ruler shows a scale of 10 pc, and the “Record” numbers indicate time in units of  $10^4$  yr. The color scheme denotes the *volume* density of the gas represented in the image, with higher transparency given to lower-density gas, so that the highest-density gas appears purple, because it is shown in red, surrounded by a layer of blue-colored material. See text for a description of the events.

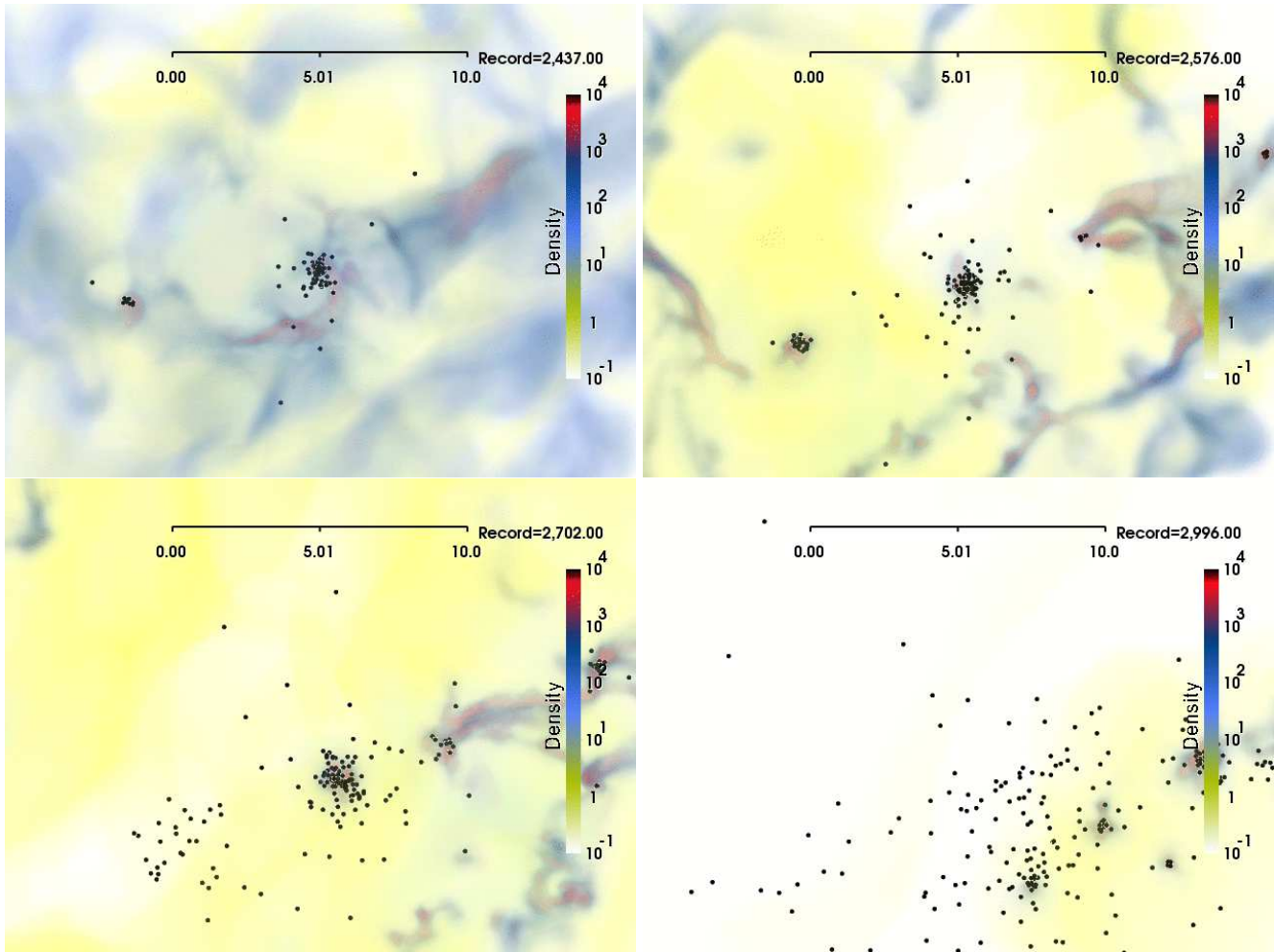


**Figure 3.** Four projected images zooming in around the intermediate-mass cluster at  $t = 24.37, 25.62, 27.02,$  and  $29.96$  Myr, showing the destruction of filament, formation of an HII region, and finally the dispersal of the gas. See text for a description of the events. Labels are as in Fig. 2.

#### 4.4 Spatial and statistical distributions of age and mass

##### 4.4.1 Age distributions and gas and star velocity dispersions

The GHC mechanism implies that each star-forming site is locally undergoing collapse while simultaneously it is falling into larger-scale potential wells. Moreover, since the small-scale regions are forming stars on their own, this process in turn implies that the larger scales are fed both gas and stars (cf. Sec. 4.1) from the surrounding infalling material. Also, the small-scale regions fall into the larger-scale ones mostly along filaments (Gómez & Vázquez-Semadeni 2014).

An important consequence of this “mixed” (gas+stars) infall is that the ensemble of stars constitutes a non-dissipative “fluid” that conserves the kinetic energy of the infalling motions. Thus, the stars formed *before* reaching the large-scale collapse center should exhibit a velocity dispersion corresponding to their motions as they were infalling to the center of the large-scale potential well. In turn, this implies that older stars should reach somewhat larger distances from the center of a group or cluster that has under-

gone mergers than the stars formed *in situ* in this merged clump, where the gas from which they inherit their velocity dispersion has probably been shocked and thus has lost some of the infall kinetic energy.

Figure 8 shows the age of the stellar particles as a function of their distance to the center of mass of Cluster 2 at  $t = 22.4$  Myr. It is seen that all of the youngest stars ( $t_{\text{age}} \lesssim 0.5$ , and in particular several stars with  $t_{\text{age}} \lesssim 0.1$  Myr), are located within the central 0.5 pc of the cluster. This is qualitatively consistent with the observation that the youngest stars appear tightly clustered around core-like or filamentary star-forming regions (e.g., Getman et al. 2014b; Povich et al. 2016, see the discussion in Sec. 5.2).

Instead, at larger distances ( $> 1$  pc), there are no particles with  $t_{\text{age}} \lesssim 1.5$  Myr. These older stars are the ones that formed in Groups 1 and 2, prior to their merging. This can also be seen in the *bottom left* panel of Fig. 4, which shows that the stars farther from the center of Group 1-2 are all represented by circles and squares (i.e., formed previously to the merger) and by green and cyan colors, denoting ages between 1 and 4 Myr, while the stars clustered near the cen-



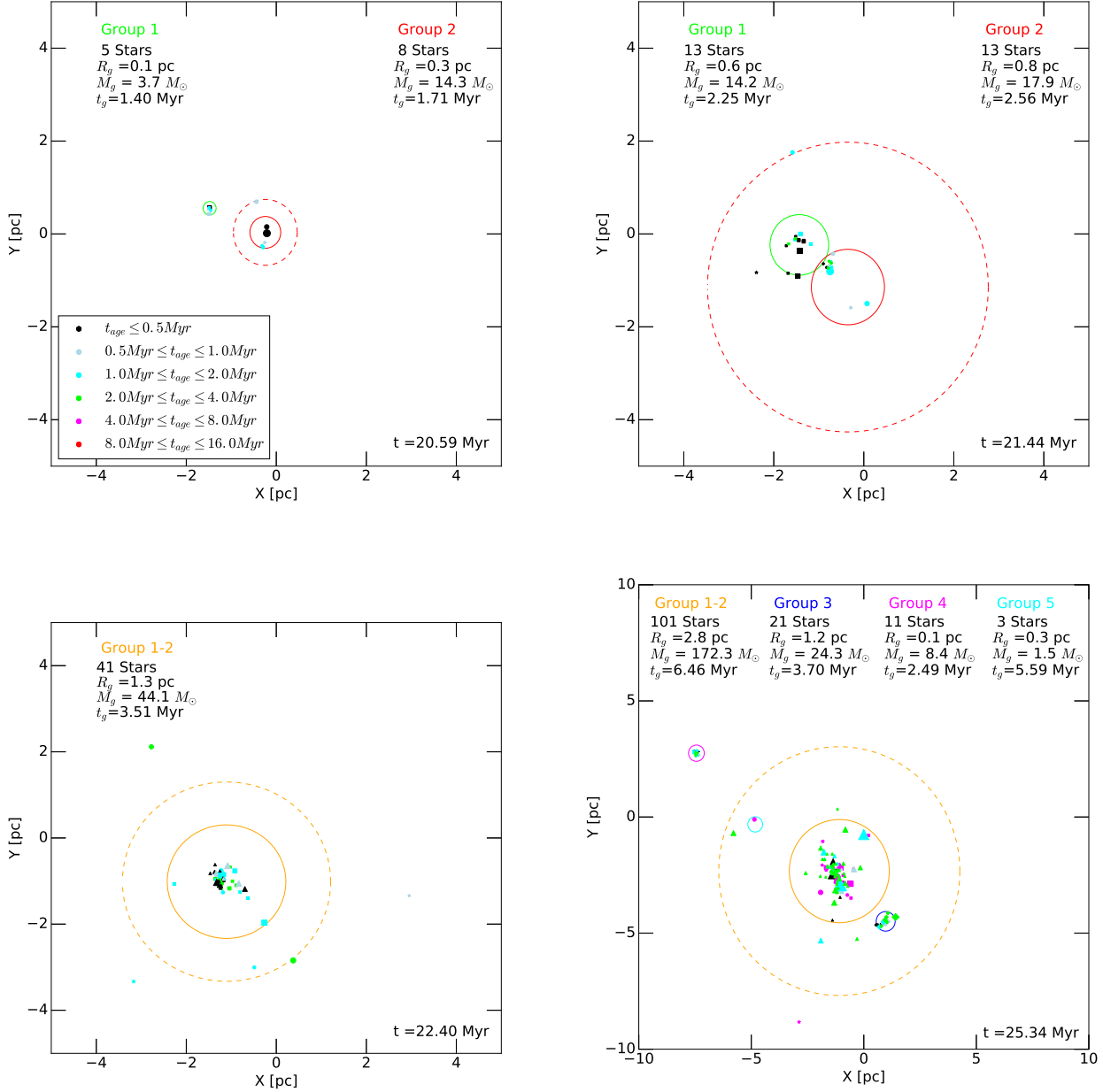


**Figure 4.** Four snapshots of “cluster 2” at times  $t = 20.59$ ,  $21.44$ ,  $22.44$  and  $25.34$  Myr in the simulation (respectively, *top left*, *top right*, *bottom left*, and *bottom right* frames), showing the merging of two sub-groups to form a larger one, while simultaneously they expand and stars continue to form in their parent clumps. Group membership is defined as described in Sec. 3. Square symbols represent stars that belong to Group 1, and filled circles represent stars belonging to Group 2. The two groups merge at  $t = 21.56$ . Triangles represent stars born in the new Group 1-2. By  $t = 25.34$  Myr, three more groups, named Groups 3, 4, and 5, are seen to have formed, lying approximately in a straight line, because they formed in the filament feeding the main clump. Colors represent stellar ages as indicated in the box in the *top left* frame. Solid circles represent the group’s size out to the most distant star, and dashed circles represent the size out to the second most distant star. Finally, the symbol sizes qualitatively represent the stellar particles’ masses.

ter have ages  $\leq 0.5$  Myr, as indicated by their black-colored symbols.

On the other hand, we also notice in Fig. 8 that the inner  $0.5$  pc of the cluster also contains several old stars, and in particular, the oldest ones ( $t_{\text{age}} \sim 2\text{--}3.5$  Myr). This suggests that some of the stars formed previously to the merger have already had  $N$ -body interactions with the other

stars in the region, and thus have transferred their excess kinetic energy to other stars in the cluster. This is facilitated because these old stars have low masses, so that they are strongly affected by interactions with more massive ones. Indeed, as discussed in Sec. 4.3 (Fig. 6), the oldest stars have masses near the peak of the IMF, which in our case is also the minimum stellar mass (cf. Sec. 2.3).

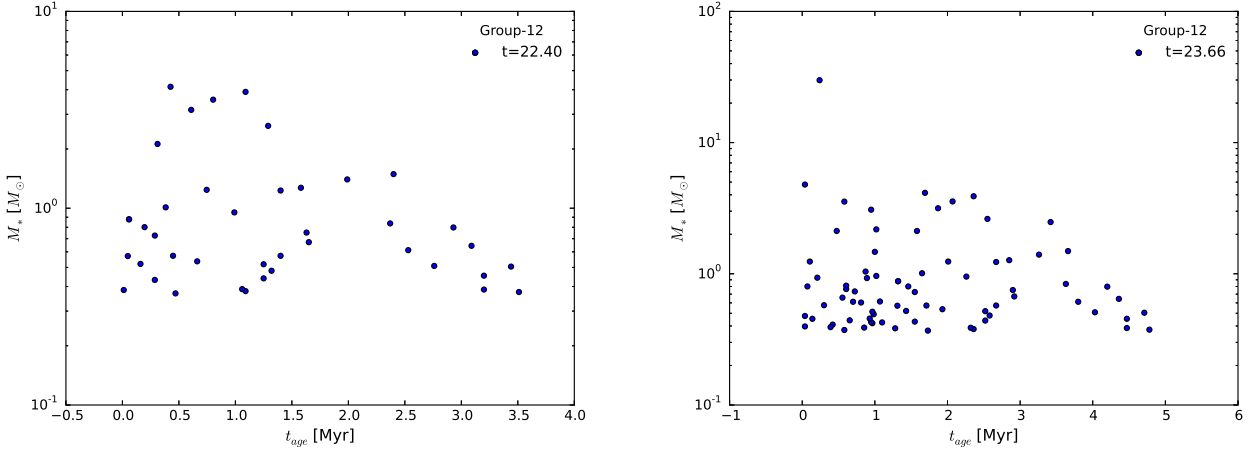


**Figure 6.** Mass *vs.* age of the cluster stars at times  $t = 22.40$  (left) and  $23.66$  Myr (right). The oldest stars are clearly seen to have masses near the minimum value. The younger stars, however, can be either young or old. Recall that the minimum mass of  $0.39M_{\odot}$  is artificially imposed by our stellar particle formation scheme.

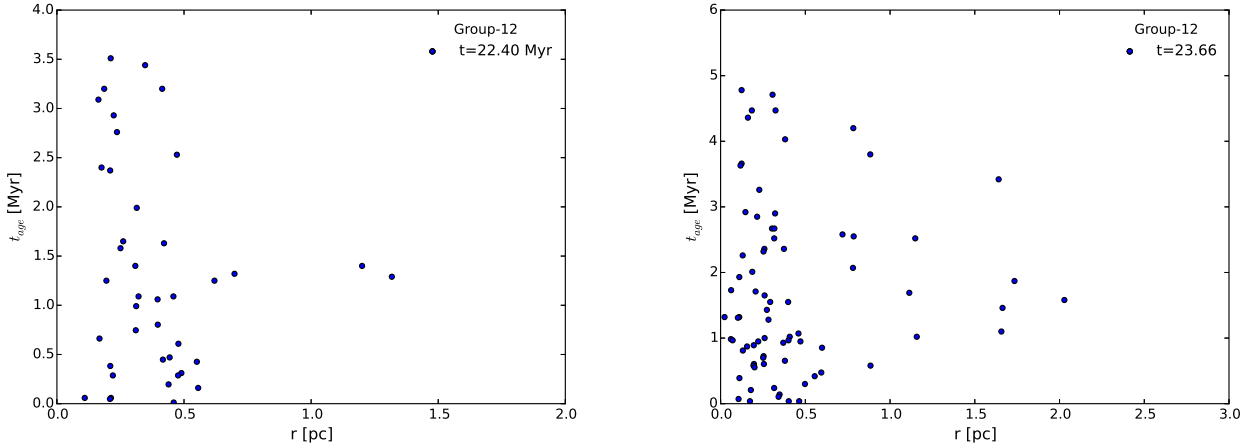


**Figure 8.** Radial age distribution of the stellar particles in the cluster at times  $t = 22.40$  and  $23.66$  Myr. At these times, the cluster is composed of the merger of Groups 1 and 2. The central  $0.5$  pc contains the youngest stars (from  $t_{\text{age}} \lesssim 0.1$  to  $0.5$  Myr), while no stars younger than  $t_{\text{age}} \approx 1$  Myr exist at radii  $r \gtrsim 0.6$  pc. The old ( $t_{\text{age}} > 2$  Myr) are those that formed in Groups 1 and 2 prior to their merger. Also, the cluster is seen to have expanded from  $t = 22.40$  to  $23.66$  Myr from a radius  $r \approx 1.4$  to  $2$  pc.

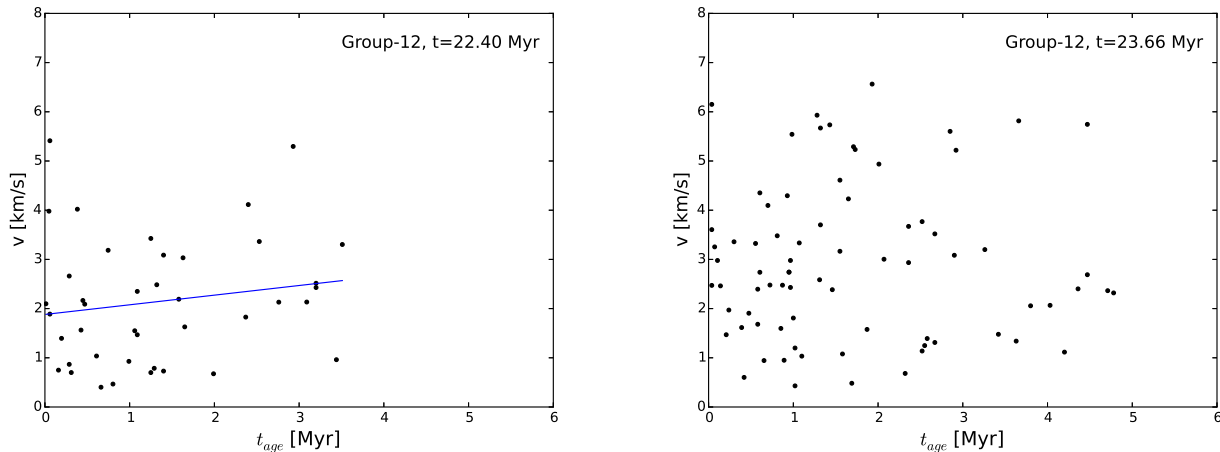
Also, as mentioned in Secs. 1 and 4.3, another implication of the GHC is that the SFR increases in each star-forming site until feedback begins to destroy the gas supply onto it, at which point the SFR begins to decline there, and perhaps shut off completely. Using a semi-analytic model for the evolution of collapsing clouds and their SFR, Zamora-Avilés et al. (2012) showed that this acceleration of the SF at each star-forming site implies that the age histogram of the site before a few Myr of its destruction is characterized by a large peak of very young (age  $< 1$  Myr) and a small tail of older (up to several Myr) stars, similarly to the age histograms of embedded clusters in various nearby MCs (Palla & Stahler 1999, 2000, 2002).

Figure 10 shows the age histogram of the stars in Groups 1 and 2 at various times, as the clumps that embed them merge and continue to form stars. At  $t = 20.44$  Myr, the two clumps and their embedded groups are still sepa-

rate, and a histogram for each group is shown. At  $t = 22.4$  Myr, the two clumps and their embedded groups have already merged, and thus a single histogram is shown. It is seen that, at this time, the most numerous stars are those less than  $1$  Myr old. Nevertheless, there are also a few stars up to nearly  $4$  Myr old. This indicates an acceleration of SF during the first  $\sim 4$  Myr of evolution of Cluster 2. At later times ( $t = 24.78$  and  $t = 25.76$  Myr), the number of young stars decreases, while the most numerous stars are those formed around  $t \approx 22.40$  Myr. This indicates a decline of the SFR after this time due to the onset of gas dispersal by the feedback.

#### 4.4.2 Mass distributions

Figure 11 shows the radial distribution of the stellar particle masses at  $t = 22.40$  Myr. It can be seen that all but one of



**Figure 9.** Stellar velocity *vs.* age for the cluster at times  $t = 22.40$  and  $23.66$  Myr. In the *left* panel, the solid line is a fit to the data points, indicating the trend of increasing velocity dispersion with larger age.

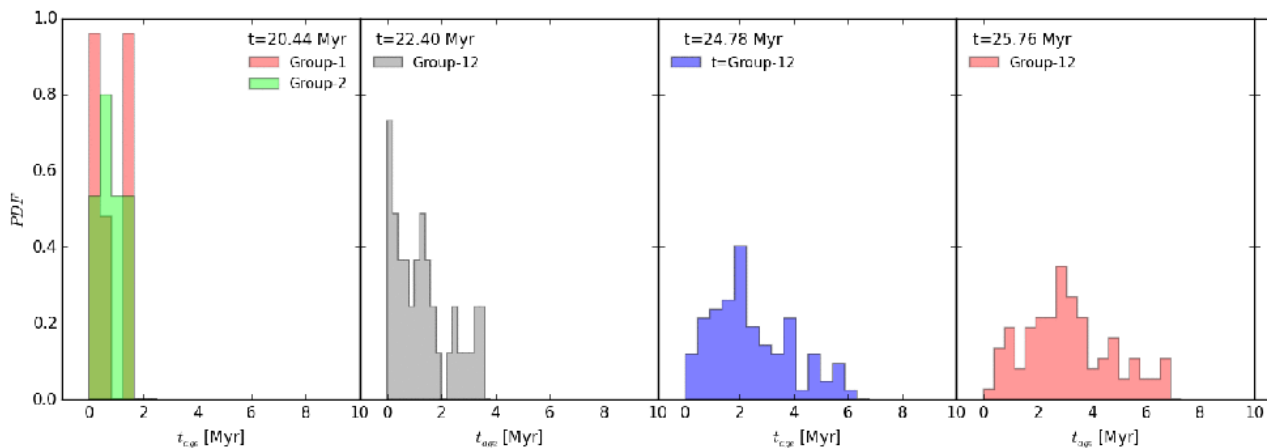


**Figure 10.** Age histogram of Cluster 2 at various times.

the stars with mass  $M > 2M_{\odot}$ , and all stars with  $M > 3M_{\odot}$  are located within  $\sim 0.5$  pc of the computed center of the cluster. Only one star with  $M \approx 2.5M_{\odot}$  is located at  $r \approx 1.3$  pc from the cluster’s center of mass. However, close inspection of the time sequence outlined by the various images of Fig. 4 shows that this is a runaway star formed in, and ejected from, Group 1 before the merger. This star is represented by the cyan squared symbol lying on the green solid circle in the *top right* panel [ $t = 21.44$  Myr] of Fig. 4 and on the solid orange circle in the *bottom left* [ $t = 22.40$  Myr] panel. Thus, this star is just “flying by” the cluster. Instead, the other massive stars in Group 1-2 have formed *in situ*, as indicated by the triangular shape of their symbols in Fig. 4.

Also, the other massive stars are represented by symbols of white and cyan colors, and with triangular shapes, indicating that those stars are younger ( $t_{\text{age}} < 2$  Myr), and formed *in situ* in the merged Group 1-2. Thus, we conclude that, except for the star that is “passing by”, the massive stars have formed after the merger of Groups 1 and 2 to form Group 1-2, thus being younger and tightly clustered near the group center.

#### 4.5 Cluster expansion

Another feature of the cluster evolution seen in Figs. 8 and 11 is that the cluster expands as it evolves, increasing its radius from  $r \approx 1.4$  pc at  $t = 22.40$  Myr to  $r \approx 2$  pc at  $t = 23.66$  Myr. The reason for this is not totally clear. It can be due in part to the fact that the gaseous material is beginning to be expelled from the clump, as can be seen in Figs. 2 and 3, and in part to the fact that the velocity dispersion of the older stars, formed in the scattered SSLA regions that have fallen into the LSSA one, corresponds to the large-scale potential well, not that of the local star-forming site (cf. Sec. 4.4.1), causing the cluster to expand to a size representative of this somewhat larger energy.

#### 4.6 Self-similar cluster structure

We now discuss the hierarchical structure of the cluster itself, resulting from the process of GHC of its parent cloud. Figure 12 shows the stars belonging to the cluster at time  $t = 29.96$  Myr, first as a whole, and then as identified by a friends-of-friends algorithm using three different values of

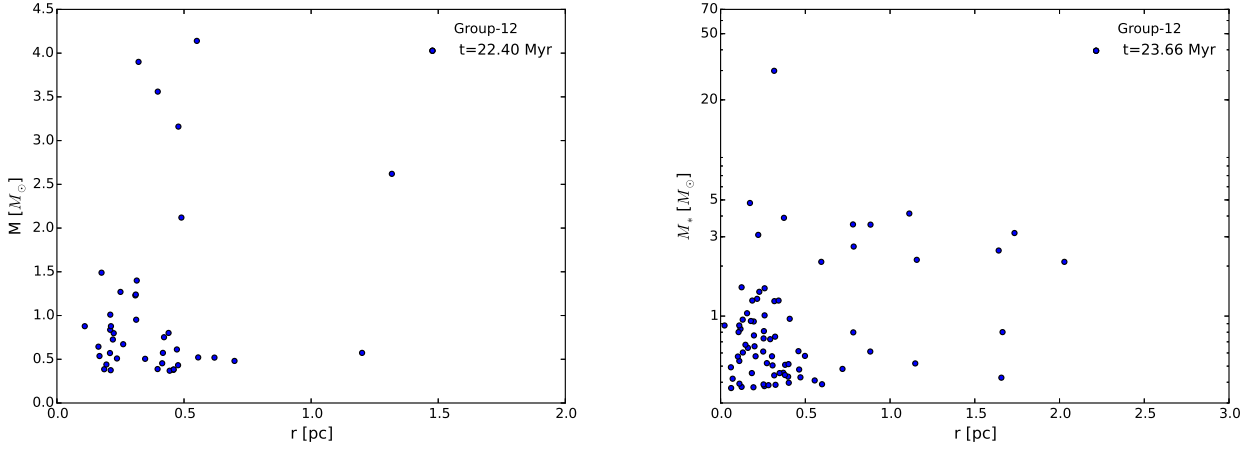


**Figure 11.** Radial distribution of the stellar particle masses at  $t = 22.40$  and  $23.66$  Myr. Note that the vertical axis is linear in the left panel, and logarithmic in the right panel.

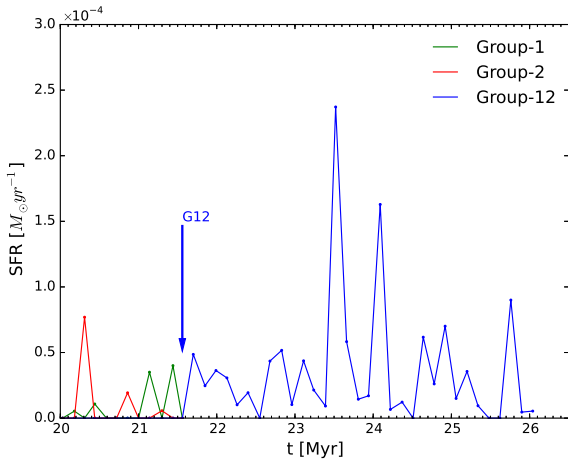


**Figure 5.** Evolution of the SFR for Groups 1, 2 and 1-2.

the “linking parameter”  $\ell$ , which determines how far neighbours are searched in order to identify a group. We see that, using a small value of the parameter ( $\ell = 0.5$ , *top right* panel), 10 tight groups are identified (denoted by the different colors), while using larger values ( $\ell = 1$  and  $2$ , *bottom left* and *bottom right* panels), respectively 9 and 4 are identified, each group being significantly more extended. We also note that, at the lowest value,  $\ell = 0.5$ , a whole group of moderately scattered stars is left out, which is nevertheless identified as a group at higher values.

These results show that the structure of the cluster resulting from the global, hierarchical contraction of the cloud, is inherently “nested”, consisting of structures within structures within structures, reflecting the structure of the parent cloud, which in turn is a consequence of its multi-scale, hierarchical collapse.

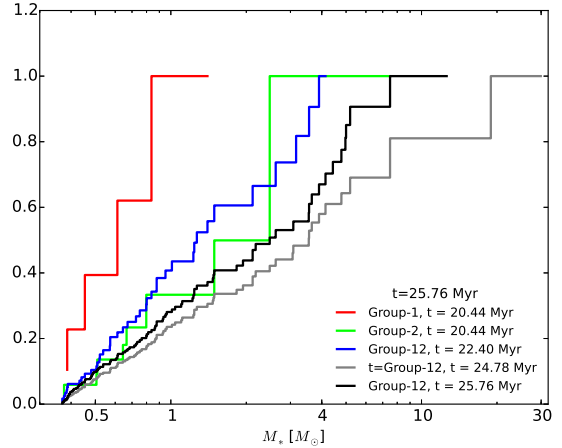


**Figure 7.** Normalized cumulative stellar mass histogram for Groups 1, 2, and 1-2 at various times. As time proceeds, a larger fraction of the stars are seen to be massive.

## 5 DISCUSSION

### 5.1 Summary of cluster properties resulting from hierarchical assembly

We can summarise the discussion in the previous section as follows. The underlying assumption for interpreting the emerging properties of the clusters formed in the scenario of GHC is that first proposed in Vázquez-Semadeni et al. (2009), namely that massive stars only form in sites where the local SFR is high enough that the IMF can be sampled to correspondingly large stellar masses. Conversely, the most common stars in low-SFR sites should be those at the peak of the IMF. This is, of course, a fully probabilistic interpretation of the IMF, and it does not address the physical mechanisms responsible for the development of the IMF itself. However, it allows a framework for understanding the assembly of the clusters.

Also, under the assumption that structures of all scales are collapsing, as required by the GHC, at a given density

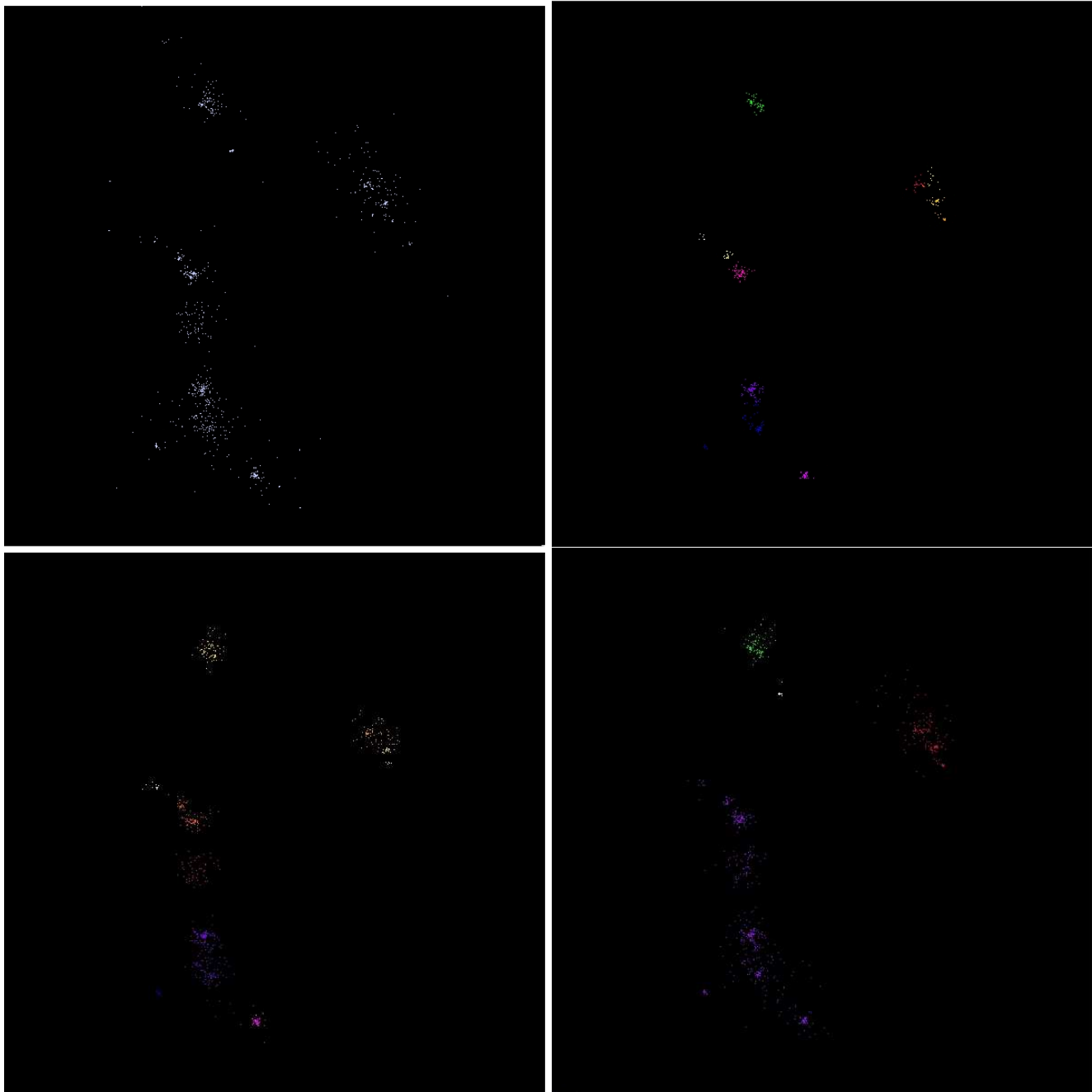


**Figure 12.** Groups identified by the Friends-of-Friends algorithm in Cluster 2 at time  $t = 29.96$  Myr varying the “linking parameter”  $\ell$  of the algorithm, which determines the distance out to which neighbours are searched. *Top left:* All stars in the cluster. *Top right:*  $\ell = 0.5$ . *Bottom left:*  $\ell = 1$ . *Bottom right:*  $\ell = 2$ .

(and therefore, a given free-fall time), more massive clumps are expected to have higher SFRs, if the SFR is given, to first order, by the ratio of the clump mass to its free-fall time.

Our simulation mimics these hypotheses, due to the probabilistic scheme used for the formation of a stellar particle. The longer it takes for a particle to form, the more massive it will be, since the cell in which it forms continues to accrete and becomes more massive, without further refinement, and then the particle forms with half the mass of the cell. But, as shown in Figure 1 of Paper I, the probability

of being able to wait very long times before forming a stellar particle is very low, and so the probability of forming of a very massive star is also very low. Thus, our simulation is expected to generally only form massive stars when the local SFR is very high, although there can be a few exceptions to this pattern.

Finally, in the GHC scenario, the low-mass, small-scale but large-amplitude (SSLA) star-forming sites should appear earlier in the evolution of the cloud, because of their shorter free-fall times, while the high-mass, larger-scale, smaller-amplitude (LSSA) sites should appear later. More-

over, the low-mass sites should be falling into the trough of the gravitational potential well of the high-mass ones. However, low-mass sites continue to appear at all times in the filaments that feed the massive clumps until the filaments are destroyed by the feedback. Thus, the low mass stars formed in the low-mass, infalling clumps share the clumps' infall velocity, and thus should have larger velocity dispersions than the stars formed in the main, massive clump, which can have both low or high masses.

The above considerations imply a number of properties of the resulting clusters:

(i) The oldest stars tend to have low masses. However, the converse is not necessarily true: low-mass stars in general can be either young or old. This trend is shown in the *top* panel of Fig. 6, which shows the mass *vs.* the age of the stars in the cluster at times  $t = 22.40$  and  $23.66$  Myr.

(ii) The oldest stars have larger velocities (Fig. 9, *left* panel), and consequently, they may be encountered at larger distances from the local star-forming site (Fig. 8).

(iii) The most massive stars appear later (a few Myr) in the evolution of the clump ensemble, when various SSLA sites have merged to form a LSSA site. This is shown in Figure 7, which gives the cumulative stellar mass histogram for Groups 1 and 2, independently and combined, at various times. As time proceeds, progressively larger fractions of the stars are seen to be massive.

(iv) The SFR increases during the early stages of the cluster assembly, until the time when massive stars begin to form. After this time, the SFR decreases, as the ionising feedback from the massive stars begins to destroy the clump and its filamentary gas supply. This is seen in the evolution of the age histogram, shown in Fig. 10.

(v) The oldest stars constitute a minority, since the SFR initially increases with time. However, after the appearance of OB stars that can partially or completely destroy the local clump and its supplying filaments, the SFR decreases again, and thus stars younger than the age of the oldest massive stars should be less abundant as well, as also shown in Fig. 10.

Note that these properties refer to regions of sizes a few parsecs and ages of at least a few Myr, and so it specifically does *not* refer to the local and instantaneous stellar production in a single clump, for which our simulation cannot discern whether massive stars form first or last, or how long does it take to build a massive star.

Also, note that young star-forming regions may consist of several low-mass local star-forming sites, and contain no large-scale site yet. This situation corresponds to times where the first low-mass sites have not yet merged to form a more massive one.

## 5.2 Comparison with observations

Our numerical results are qualitatively consistent with recent observational results on the age and mass distributions of young stellar objects in star-forming regions. In particular, Getman et al. (2014a,b) have recently reported the existence of age gradients in the stellar populations of various massive star-forming regions, such that the youngest stellar objects are located in the obscured regions of molecular

clouds, intermediate-age objects are located in revealed clusters, and the oldest objects are found in distributed populations. This is qualitatively consistent with our result that the oldest objects can be found at large distances from the cluster's center due to their larger velocity dispersion, in turn due to their formation far from it, so that their velocities include the component from their infall onto the central massive clump. Instead, younger objects formed in the clump lack this component of the velocity, and these are characterised by somewhat lower velocities. Also, the larger velocity dispersion of the older objects predicted by the GHC scenario has been observed by Mairs et al. (2016) in the Orion A cloud.

Getman et al. (2014b) considered several possible scenarios that could lead to the age segregation they observed. Of these, the one closest to the mechanism of hierarchical assembly by GHC is their scenario B, since it invokes the acceleration of SF as proposed by Palla & Stahler (2000), which is consistent with our scenario (Zamora-Avilés et al. 2012). However, the similarity between GHC and Scenario B of Getman et al. (2014b) is not complete, since they did not consider the accretion of both stars and gas onto the trough of the large-scale potential well.

In addition, Povich et al. (2016) have concluded that the cloud complex known as the M17 southwest extension (M17 SWex) appears to be lacking very massive stars in comparison with the number expected from its estimated SFR. This region consists of several scattered star-forming cores, separated by distances of several parsecs from each other (M. Povich, private communication; see also Busquet et al. 2013). This is consistent with the hierarchical assembly of the cluster in our simulation, since several isolated, intermediate-mass star-forming clumps may produce a relatively numerous combined population of YSOs that may however not yet have formed massive stars, because in the GHC scenario this only occurs after these smaller regions have merged to form a massive one. This is again illustrated in Fig. 7, which shows that the relative abundance of massive stars increases over time, especially after Groups 1 and 2 have merged.

We conclude that the scenario of GHC provides an assembly mechanism for clusters that naturally predicts the observed age segregation and bottom-heavy IMF of young clusters. In a future contribution we plan to carry out a detailed quantitative comparison between the clusters in simulations that sample the IMF to lower masses (see Sec. 5.3) and the observed properties of specific clusters.

## 5.3 Limitations and impact

The present study is based on the underlying hypothesis that our probabilistic stellar particle formation scheme mimics the mechanism leading to the development of the IMF. That is, we interpret the IMF strictly as a random sampling process, so that the scarcity of massive stars is interpreted to imply that the probability of forming one is very low and given precisely by the IMF. Interestingly, the fact that our simulation, using a probabilistic criterion for the formation of stellar particles (cf. Sec. 2.3), qualitatively reproduces several observed properties of young clusters, suggests that our underlying assumption is reasonably realistic.

Nevertheless, our star formation scheme does have some



limitations. Most importantly, as described in Sec. 2.3, the minimum stellar-particle mass is  $0.39M_{\odot}$ , which is near the peak of the observed stellar IMF, and thus we are missing stars on the low-mass side of the IMF. Our imposed IMF is thus a strict power law, that lacks the turnover at low masses.

This implies that we are missing a significant number of low-mass stars, about half of the total number of stars. Their mass,  $\sim 26\%$  of the total mass for a Kroupa (2001) IMF, and  $\sim 19\%$  for a Chabrier (2003) IMF, is instead deposited into the stars that do form in the simulation, with masses  $0.39M_{\odot}$  to  $61M_{\odot}$ . This may affect the dynamics of the clusters formed in the simulation, although not very strongly, since the missing stars have low masses, and are not expected to affect the dynamics of the higher-mass ones too much, especially if they tend to form a roughly uniform background. The fact that the structure of our clusters resembles that of observed young clusters reinforces this expectation. We nevertheless plan to improve our star formation scheme in order to produce a more complete stellar-particle mass spectrum, and with this carry out a more detailed and quantitative comparison with observations. Meanwhile, we consider that our study conveys an illustrative first approximation to the problem of cluster assembly, capturing the essential aspects of the hierarchical assembly of these objects.

Other limitations of our simulation are that it does not include magnetic fields nor any form of feedback other than ionisation heating, in particular supernova (SN) explosions. The neglect of magnetic fields may not be crucial, since our present understanding is that MCs are generally magnetically supercritical, meaning that the magnetic field is in general unable to support them against their own self-gravity (e.g., Crutcher 2012), and therefore they proceed unimpeded to global collapse.

The neglect of SN explosions is also not crucial because of two main reasons. First, it is becoming increasingly accepted that SN explosions need to occur within the clouds in order to remove significant amounts of mass from the clouds (Iffrig & Hennebelle 2015), although on the other hand, only SNe that explode in low-density environments avoid energy losses that allow efficient coupling with the gas (Girichidis et al. 2016). Also, pre-SN feedback is required to allow blastwaves to propagate efficiently into the ISM (Geen et al. 2016). Second, and more importantly, our study suggests that the assembly of the clusters is accomplished mostly during the early stages (first few Myr) of the clouds' evolution, during which few or no SNe are expected to occur, especially if massive stars form late in the evolution of the cloud, as suggested by the GHC scenario. So, the ionising feedback included in our simulations is probably the most relevant form of feedback for regulating the gas flow onto the sites where the new stars are forming.

Finally, our feedback prescription (Sec. 2.4) is of course crude, solving the radiative transfer only in an approximate way. Although it was shown in Paper I that the evolution of an HII region with this prescription does track the uniform-medium analytic solution reasonably well, it is possible that our prescription allows evaporation of regions that should be shaded behind dense clumps, since it does not take into account the density of the intervening material between the ionising star and the cell on which the effect of the radiation is being determined. Thus, our simulations may somewhat

overestimate the evaporation rate of material in filaments containing dense clumps. However, since the filaments themselves are denser than the background medium, and their length far exceeds that of isolated clumps and cores, their column density for situations where the filament is aligned with the ionising object and with the intervening clump (as in the case of filaments feeding the main clump where the ionising object formed) may be comparable to or even larger than that of the intervening clump. Therefore, the shadowing caused by this clump is likely to be of secondary importance. Indeed, Figure 10 in Paper I shows the gradual evaporation of filaments containing clumps in a way that allows the formation of “pillars”, and finally isolated globules within growing HII regions, similarly to objects like the “Pillars of Creation” and dark globules, respectively. On the other hand, our feedback prescription allows the simulations to run orders of magnitude faster than if the radiative transfer is followed in full. We thus conclude that our prescription provides a sufficiently realistic framework for the study of the assembly of stellar clusters.

## 6 SUMMARY AND CONCLUSIONS

In this paper, we have discussed the mechanism of assembly of a cluster in a numerical simulation of cloud formation and collapse by converging flows. The assembly proceeds in a hierarchical way as a consequence of the hierarchical nature of the collapse of its parent cloud (Vázquez-Semadeni et al. 2009). The hierarchical collapse regime consists of small-scale, large-amplitude (SSLA) collapses (involving small total masses) within large-scale, small-amplitude (LSSA) ones (involving large masses, which are spread out over large scale regions). Collapse at all scales involves accretion onto the troughs of the potential wells (the collapse “centers”). The large-scale collapses involve the generation of filamentary flows that funnel material from the whole large-scale region down to its collapse center, and the small-scale collapsing regions “ride” along these large-scale filamentary flows (Gómez & Vázquez-Semadeni 2014), in a “conveyor belt” fashion (Longmore et al. 2014). Because the small-scale collapses start forming stars earlier (due to their larger amplitudes, which imply shorter free-fall times), they often reach the large-scale collapse center already containing stars in addition to fresh gas.

This mechanism then implies that massive star-forming sites form by the merging of smaller-scale star-forming regions, which supply both stars and gas to the larger sites, and thus these larger-scale sites contain a mixture of locally formed stars and stars that formed at a remote, smaller-scale site and that are brought to the large-scale site by the infalling flow. Moreover, the stars that form in the small-scale, scattered sites have an infall velocity corresponding to the larger-scale potential well. However, stars formed in the massive center of the large-scale collapse, form from gas that has probably been shocked upon its arrival there, and so they form with a somewhat lower velocity dispersion.

Finally, this scenario also implies that the SFR must increase with time during early stages of evolution, and then decrease again as the massive stars begin to destroy their forming sites (Zamora-Avilés et al. 2012). This acceleration of the SF process, combined with a face-value interpretation

of the IMF as a probability distribution function of stellar masses, suggests that massive stars are only expected to form once the SFR is large enough to sample the IMF to high masses. Therefore, massive stars should form last in the evolution of the whole ensemble of star-forming sites, once the low-mass ones have merged to form a large-mass, high-SFR one.

From these considerations, we have concluded that a cluster that has formed from the hierarchical collapse of its parent cloud must have the following characteristics:

- The oldest stars tend to have low masses, because they formed in the low-mass sites early in the evolution of the cloud. However, newer stars can be either low-or high mass, as they form in the high-mass site formed by the merger of the low-mass ones.
- The oldest stars tend to have larger velocity dispersions, because they are characterized by the infall velocity of the material onto the high-mass collapse center. However, this effect tends to be washed out by the stellar interaction as the cluster ages.
- As a consequence, older stars tend to be at larger distances from the collapse center (or filament).
- The most massive stars tend to be younger, because they only form when the SFR of the whole region has increased sufficiently to sample the high-mass regions of the IMF.
- As a consequence, the low- and intermediate-mass sites that have not concluded the merging process may be deficient in the highest-mass stars.
- Because of the increasing SFR, most stars are young, although a small fraction may be as old as several Myr.

These features are in good qualitative agreement with observed properties of young clusters, which seem to have a hierarchical structure (Portegies Zwart et al. 2010, and references therein), have an age gradient, so that the oldest stars tend to be farther from the forming sites (Getman et al. 2014a,b) and to have larger velocities (Mairs et al. 2016). Also, the scenario implies that ensembles of cores in early phases of evolution will be deficient in massive stars compared to the expected number from their combined stellar production, as observed by Povich et al. (2016). We conclude that the scenario of GHC allows a clear understanding of the properties of young clusters, in terms of the multi-scale collapse of their parent clouds.

## ACKNOWLEDGMENTS

E.V.-S. is glad to acknowledge enlightening discussions with Matt Povich on the observed structure of young clusters. A.G.S. was supported by UC-MEXUS Fellowship.

## REFERENCES

Allison, R. J., Goodwin, S. P., Parker, R. J., et al. 2009, *ApJL*, 700, L99  
 Ballesteros-Paredes, J., Klessen, R. S., Mac Low, M.-M., & Vázquez-Semadeni, E. 2007, *Protostars and Planets V*, 63  
 Bate, M. R. 2009, *MNRAS*, 392, 590  
 Bate, M. R. 2009, *MNRAS*, 392, 1363

Bate, M.R., Bonnell, I.A., Price, N.M., 1995, *MNRAS*, 277, 362  
 Bate, M. R., Bonnell, I. A., & Bromm, V. 2003, *MNRAS*, 339, 577  
 Bertoldi, F., & McKee, C. F. 1992, *ApJ*, 395, 140  
 Bressan, A., Fagotto, F., Bertelli, G., & Chiosi, C. 1993, *A&AS*, 100, 647  
 Bressert, E., Bastian, N., Gutermuth, R., et al. 2010, *MNRAS*, 409, L54  
 Busquet, G., Zhang, Q., Palau, A., et al. 2013, *ApJL*, 764, L26  
 Chabrier, G. 2003, *PASP*, 115, 763  
 Clark, P. C., & Bonnell, I. A. 2005, *MNRAS*, 361, 2  
 Colín, P., Vázquez-Semadeni, E. & Gómez, G.C. 2013, *MNRAS*, 435, 1701 (Paper I)  
 Crutcher, R. M. 2012, *ARA&A*, 50, 29  
 Dale, J. E., Ercolano, B., & Bonnell, I. A. 2012, *MNRAS*, 424, 377  
 Dale, J. E., Ercolano, B., & Bonnell, I. A. 2013, *MNRAS*, 430, 234  
 Dale, J. E., Ercolano, B., & Bonnell, I. A. 2015, *MNRAS*, 451, 987  
 Dale, J. E., Ngoumou, J., Ercolano, B., & Bonnell, I. A. 2013, *MNRAS*, 436, 3430  
 Dale, J. E., Ngoumou, J., Ercolano, B., & Bonnell, I. A. 2014, *MNRAS*, 442, 694  
 Davis, M., Efstathiou, G., Frenk, C. S., & White, S. D. M. 1985, *ApJ*, 292, 371  
 Diaz-Miller, R. I., Franco, J., & Shore, S. N. 1998, *ApJ*, 501, 192  
 Federrath, C., & Klessen, R. S. 2012, *ApJ*, 761, 156  
 Federrath, C., Banerjee, R., Clark, P.C., & Klessen, R.S. 2010, *ApJ*, 713, 269  
 Franco, J., Shore, S. N., & Tenorio-Tagle, G. 1994, *ApJ*, 436, 795  
 Gao, Y., & Solomon, P. M. 2004, *ApJ*, 606, 271  
 Gatto, A., Walch, S., Naab, T., et al. 2016, arXiv:1606.05346  
 Geen, S., Hennebelle, P., Tremblin, P., & Rosdahl, J. 2016, arXiv:1607.05487  
 Getman, K. V., Feigelson, E. D., Kuhn, M. A., et al. 2014, *ApJ*, 787, 108  
 Getman, K. V., Feigelson, E. D., & Kuhn, M. A. 2014, *ApJ*, 787, 109  
 Girichidis, P., Walch, S., Naab, T., et al. 2016, *MNRAS*, 456, 3432  
 Gómez, G. C., & Vázquez-Semadeni, E. 2014, *ApJ*, 791, 124  
 Hacar, A., Alves, J., Forbrich, J., et al. 2016, *A&A*, 589, A80  
 Hartmann, L., Ballesteros-Paredes, J., & Heitsch, F. 2012, *MNRAS*, 420, 1457  
 Heitsch, F., Burkert, A., Hartmann, L. W., Slyz, A. D., & Devriendt, J. E. G. 2005, *ApJL*, 633, L113  
 Hennebelle, P., & Chabrier, G. 2011, *ApJL*, 743, L29  
 Hillenbrand, L. A., & Hartmann, L. W. 1998, *ApJ*, 492, 540  
 Hoyle, F. 1953, *ApJ*, 118, 513  
 Iffrig, O., & Hennebelle, P. 2015, *A&A*, 576, A95  
 Jappsen, A.-K., Klessen, R. S., Larson, R. B., Li, Y., and Mac Low, M.-M. 2005, *A&AS*, 173, 611  
 Kim, J., & Ryu, D. 2005, *ApJL*, 630, L45

- Kirk, H., Offner, S. S. R., & Redmond, K. J. 2014, *MNRAS*, 439, 1765
- Klessen, R. S., & Burkert, A. 2000, *ApJS*, 128, 287
- Klessen, R. S., & Burkert, A. 2001, *ApJ*, 549, 386
- Koyama, H. & Inutsuka, S.-I. 2000, *ApJ*, 532, 980
- Koyama, H., & Inutsuka, S.-i. 2002, *ApJL*, 564, L97
- Kravtsov, A. V., Klypin, A. A., & Khokhlov, A. M. 1997, *ApJS*, 111, 73
- Kravtsov, A.V. 2003, *ApJ(Letters)*, 590, 1
- Kroupa, P. 2001, *MNRAS*, 322, 231
- Krumholz, M. R., Cunningham, A. J., Klein, R. I., & McKee, C. F. 2010, *ApJ*, 713, 1120
- Krumholz, M. R., Klein, R. I., & McKee, C. F. 2012, *ApJ*, 754, 71
- Kuhn, M. A., Getman, K. V., & Feigelson, E. D. 2015a, *ApJ*, 802, 60
- Kuhn, M. A., Feigelson, E. D., Getman, K. V., et al. 2015b, arXiv:1507.05653
- Lada, C. J., & Lada, E. A. 2003, *ARA&A*, 41, 57
- Lee, Y.-N., & Hennebelle, P. 2016, *A&A*, 591, A30
- Longmore, S. N., Kruijssen, J. M. D., Bastian, N., et al. 2014, Protostars and Planets VI, 291
- Mac Low, M.-M., & Klessen, R. S. 2004, Reviews of Modern Physics, 76, 125
- Mairs, S., Johnstone, D., Kirk, H., et al. 2016, *MNRAS*, 461, 4022
- Matzner, C. D. 2002, *ApJ*, 566, 302
- McMillan, S. L. W., Vesperini, E., & Portegies Zwart, S. F. 2007, *ApJL*, 655, L45
- Moeckel, N., & Bonnell, I. A. 2009, *MNRAS*, 400, 657
- Morau, E. 2016, arXiv:1607.00027
- Palla, F., & Stahler, S. W. 1999, *ApJ*, 525, 772
- Palla, F., & Stahler, S. W. 2000, *ApJ*, 540, 255
- Palla, F., & Stahler, S. W. 2002, *ApJ*, 581, 1194
- Portegies Zwart, S. F., McMillan, S. L. W., & Gieles, M. 2010, *ARA&A*, 48, 431
- Povich, M. S., Townsley, L. K., Robitaille, T. P., et al. 2016, arXiv:1604.06497
- Rivera-Gálvez, S., Román-Zúñiga, C. G., Jiménez-Bailón, E., et al. 2015, *AJ*, 150, 191
- Salpeter, E. E. 1955, *ApJ*, 121, 161
- Spitzer, L. 1978, Physical Processes in the Interstellar Medium (New York:Wiley)
- Truelove, J. K., Klein, R. I., McKee, C. F., Holliman, J. H., II, Howell, L. H., & Greenough, J. A. 1997, *ApJL*, 489, L179
- Vázquez-Semadeni E., Gómez G. C., Jappsen A. K., Ballesteros-Paredes J., González R. F., Klessen R. S., 2007, *ApJ*, 657, 870
- Vázquez-Semadeni, E., Gómez, G. C., Jappsen, A.-K., Ballesteros-Paredes, J., & Klessen, R. S. 2009, *ApJ*, 707, 1023
- Vázquez-Semadeni, E., Colín, P. Gómez, G.C., Ballesteros-Paredes, J., & Watson, A.W. 2010, *ApJ*, 715, 1302
- Zamora-Avilés, M., Vázquez-Semadeni, E., & Colín, P. 2012, *ApJ*, 751, 77
- Zamora-Avilés, M., & Vázquez-Semadeni, E. 2014, *ApJ*, 793, 84